

G. R. Liu · K. Y. Dai · X. Han · Y. Li

A mesh-free minimum length method for 2-D problems

Received: 7 March 2005 / Accepted: 18 August 2005 / Published online: 19 October 2005
© Springer-Verlag 2005

Abstract A mesh-free minimum length method (MLM) has been proposed for 2-D solids and heat conduction problems. In this method, both polynomials as well as modified radial basis functions (RBFs) are used to construct shape functions for arbitrarily distributed nodes based on minimum length procedure, which possess Kronecker delta property. The shape functions are then used to formulate a mesh-free method based on weak-form formulation. Both Gauss integration (GI) and stabilized nodal integration (NI) are employed to numerically evaluate Galerkin weak form. The numerical examples show that the MLM achieves better accuracy than the 4-node finite elements especially for problems with steep gradients. The method is easy to implement and works well for irregularly distributed nodes. Some numerical implementation issues for MLM are also discussed in detail.

Keywords Mesh-free method · Meshless method · Minimum length method · Radial basis function (RBF) · Interpolation function

1 Introduction

Mesh-free methods have achieved remarkable progress in recent years to avoid the problems related to the creation and application of predefined meshes in the traditional numerical methods, such as the finite element method (FEM), the finite difference method (FDM). In general mesh-free methods developed so far can be categorized into three main groups. The first group includes mesh-free methods based on strong-form equations, in which discretization is formed directly

from governing differential equations, such as the smooth particle hydrodynamics (SPH) method [6, 13], the general finite difference method [9] and other mesh-free collocation methods. The second group covers the mesh-free methods based on weak-form formulation, such as element-free Galerkin (EFG) method [2], reproducing kernel particle methods (RKPM) [15], meshless local Petrov-Galerkin (MLPG) method [1], radial point interpolation method (RPIM) [10, 17] and other boundary-type mesh-free methods. The third category involves mesh-free methods combining both weak- and strong-form formulations, such as the newly developed mesh-free weak-strong form method [11, 14].

One attractive feature of strong-form methods is the high computational efficiency as no numerical integration is required. However, straightforward imposition of Neumann boundary condition often leads to unstable results. By comparison, mesh-free weak-form methods can usually achieve higher accuracy than strong-form methods especially in dealing with problems in solids and structural mechanics. In addition, they can treat Neumann boundary condition more easily and the results are more stable. Hence weak-form method is considered in this work. One of the most important issues in mesh-free methods is the construction of mesh-free shape functions. The developed shape functions should have some primary merits, such as desirable accuracy, very easy to implement, valid and stable for arbitrary nodal distribution. There are two widely used methods: moving least-squares (MLS) method and radial point interpolation method (RPIM). One successful application of MLS is its integration in the so-called EFG method [2]. EFG is a viable method which has very good accuracy and convergence rate and a high resolution of localized gradient can be achieved. As the MLS uses excessive nodes which leads to shape function lacking in delta function property. Hence its approximation function does not pass through the data points, which consequently complicate the imposition of essential boundary conditions. RPIM based on weak form was then proposed to overcome this difficulty (see, e.g., [17]). This method uses radial basis functions (RBFs) augmented with polynomials to interpolate the data points exactly and the generated shape functions pos-

G. R. Liu (✉) · K. Y. Dai · Y. Li
Center for ACES, Department of Mechanical Engineering,
National University of Singapore, Singapore 119260, Singapore
E-mail: mpeliugr@nus.edu.sg
Tel.: +65-6874 6481
Fax: +65-6779 1459

X. Han
College of Mechanical and Automobile Engineering,
Hunan University, Changsha 410082, P. R. China

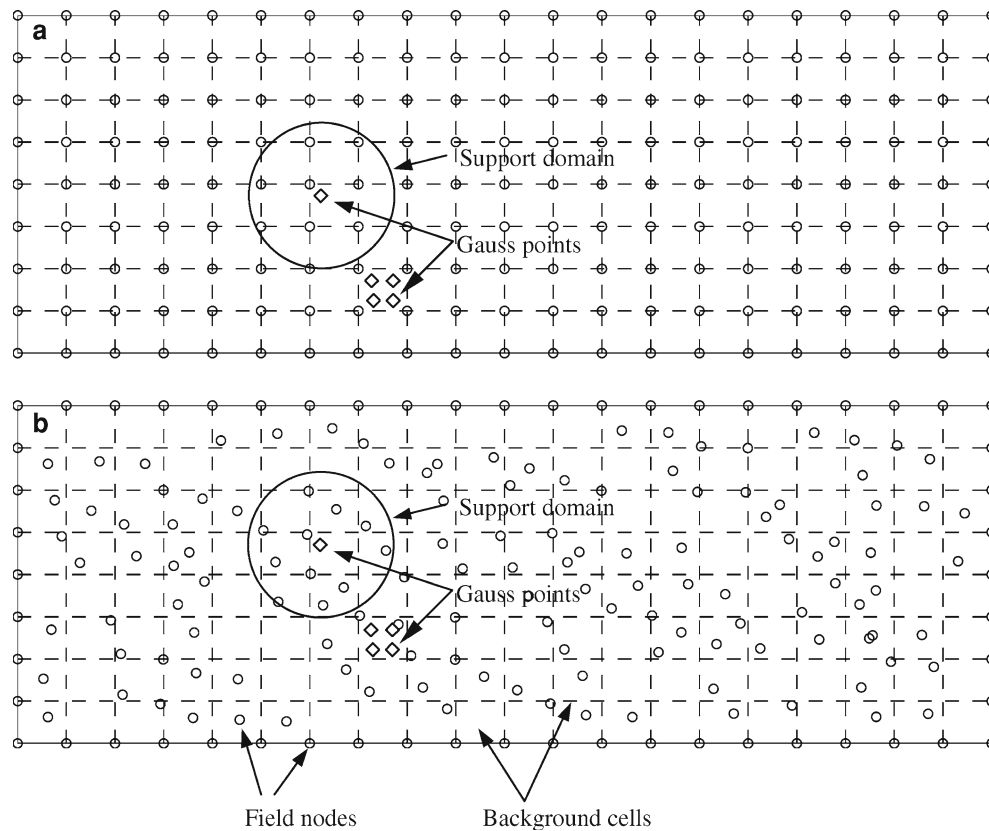


Fig. 1 Nodal arrangements and background cells for the cantilever beam when using Gauss integration. (a) Regular and (b) irregular nodal distribution

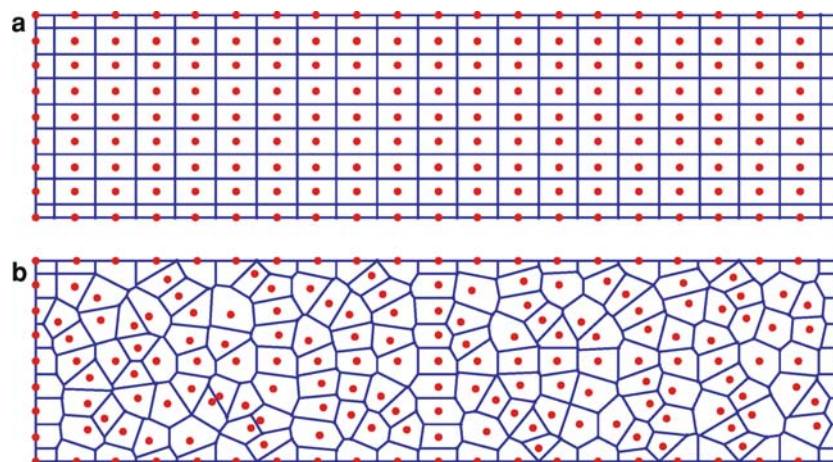


Fig. 2 Domain discretization using Voronoi diagram for nodal integration. (a) Regular and (b) irregular nodal distribution

sess the delta function property. The method uses exactly the same number of interpolation bases as the nodes in support domain and the selected bases are predetermined before analysis.

In this paper a mesh-free minimum length method (MLM) is presented to construct shape functions for a set of scattered nodes. Some polynomial terms combined with modified RBFs are used to interpolate field nodes. As the number of interpolation bases (polynomials plus RBFs) is larger than

the sampling nodes in the adopted functional, the minimum length procedure is employed to determine unknown coefficients and then the shape functions are obtained. It will be proved that these shape functions possess the delta function property. The MLM shape functions are then used to establish a mesh-free method based on weak form formulation for 2-D elasticity problems (termed as MLM in short). Both Gauss integration and stabilized nodal integration are employed to evaluate the Galerkin weak form. Some numerical

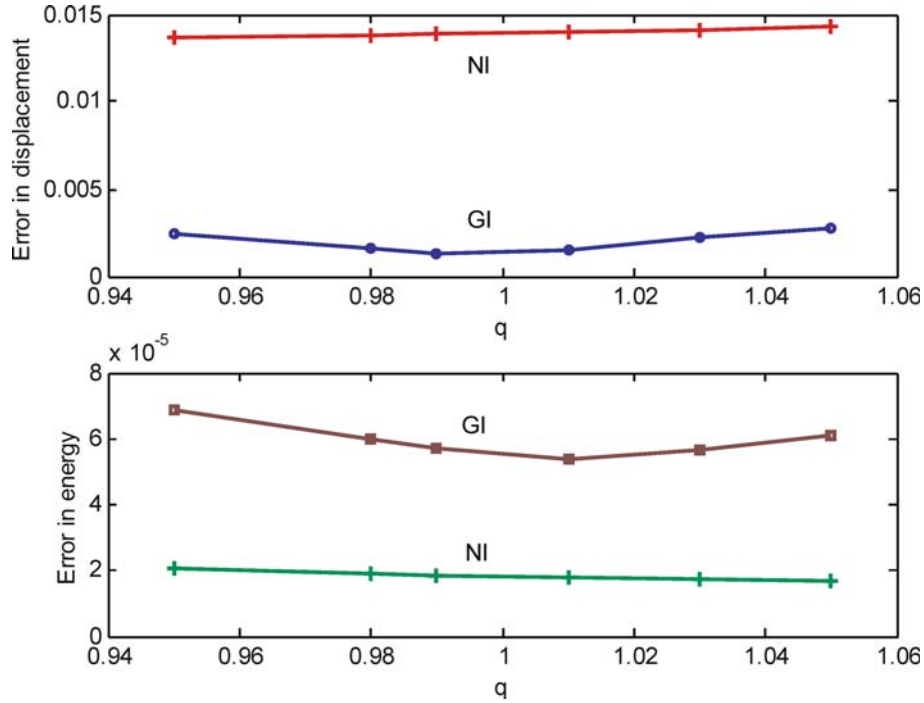


Fig. 4 Error distributions in (a) displacement norm and (b) energy norm using different shape parameter q 's

Hence

$$\phi_i(\mathbf{x}_j) = \{\mathbf{b}(\mathbf{x}_j)\mathbf{B}_0^T[\mathbf{B}_0\mathbf{B}_0^T]^{-1}\}_i = \begin{cases} 1 & (i = j) \\ 0 & (i \neq j) \end{cases} \quad (11)$$

This indicates that the MLM shape functions are exact interpolators. Hence the essential boundary conditions can be enforced directly as in the conventional FEM.

2.2 Comparison with the RPIM

Both MLM and RPIM construct their shape functions using RBFs along with some monomial terms and their derived shape functions have delta properties. RPIM can be established from either the direct interpolation concept [17] or the moving Kriging method [5]. As MLM and RPIM are formulated from different mathematical backgrounds, their shape functions accordingly differ in expressions.

The RPIM shape functions are given in the form below (see [10] for details).

$$\Phi = \mathbf{r}^T \mathbf{S}_a + \mathbf{p}^T \mathbf{S}_b \quad (12)$$

where

$$\mathbf{S}_b = [\mathbf{P}_m^T \mathbf{R}_Q^{-1} \mathbf{P}_m]^{-1} \mathbf{P}_m^T \mathbf{R}_Q^{-1} \quad (13)$$

$$\mathbf{S}_a = \mathbf{R}_Q^{-1} [\mathbf{1} - \mathbf{P}_m \mathbf{S}_b] \quad (14)$$

$$[\mathbf{R}_Q]_{i,j} = r_j(\mathbf{x}_i); \quad (i, j = 1, 2, \dots, n) \quad (15)$$

$$[\mathbf{P}_m]_{i,j} = p_j(\mathbf{x}_i); \quad (i = 1, \dots, n; j = 1, \dots, n_p), \quad p_0 = 1 \quad (16)$$

Comparing the MLM shape functions with those of RPIM, one can see that the former have a simpler form. Furthermore, if we examine the work of matrix manipulations, RPIM needs to determine the inverse of two matrices with sizes $(n \times n)$ and $(n_p \times n_p)$, respectively, whereas in MLM only the first inverse is required. In addition, when calculating the shape functions at one quadrature point, RPIM needs to perform $n^2(n + 4n_p + 1) + nn_p(n_p + 1)$ times of multiplication while MLM needs $n(n + n_p)(2n + 1)$ times. Subtraction the second from the first leads to the conclusion that, if

$$n > (1 + \sqrt{2})n_p \quad (17)$$

or in more detail, if $n > 7.2$ for $n_p = 3$ (Linear polynomials) and $n > 14.4$ for $n_p = 6$ (Quadratic polynomials), the computational work for RPIM is larger than for MLM. These conditions are often satisfied in general practice. On the whole, RPIM is computationally more expensive than MLM. However, the main drawback of MLM is the loss of linear reproduction property as compared to RPIM.

3 Integration of weak form

A 2-D problem in solid mechanics can be described by equilibrium equation in the domain Ω bounded by Γ and $\Gamma = \Gamma_u + \Gamma_t$, $\Gamma_u \cap \Gamma_t = \emptyset$. Note that the inertia effect is not considered here.

$$\sigma_{ij,j} + b_i = 0 \quad \text{in } \Omega \quad (18)$$

where σ_{ij} is the component of stress tensor and b_i is the body force component. Boundary conditions are given as follows.

$$\sigma_{ij}n_j = \bar{t}_i \quad \text{on } \Gamma_t \quad (19)$$

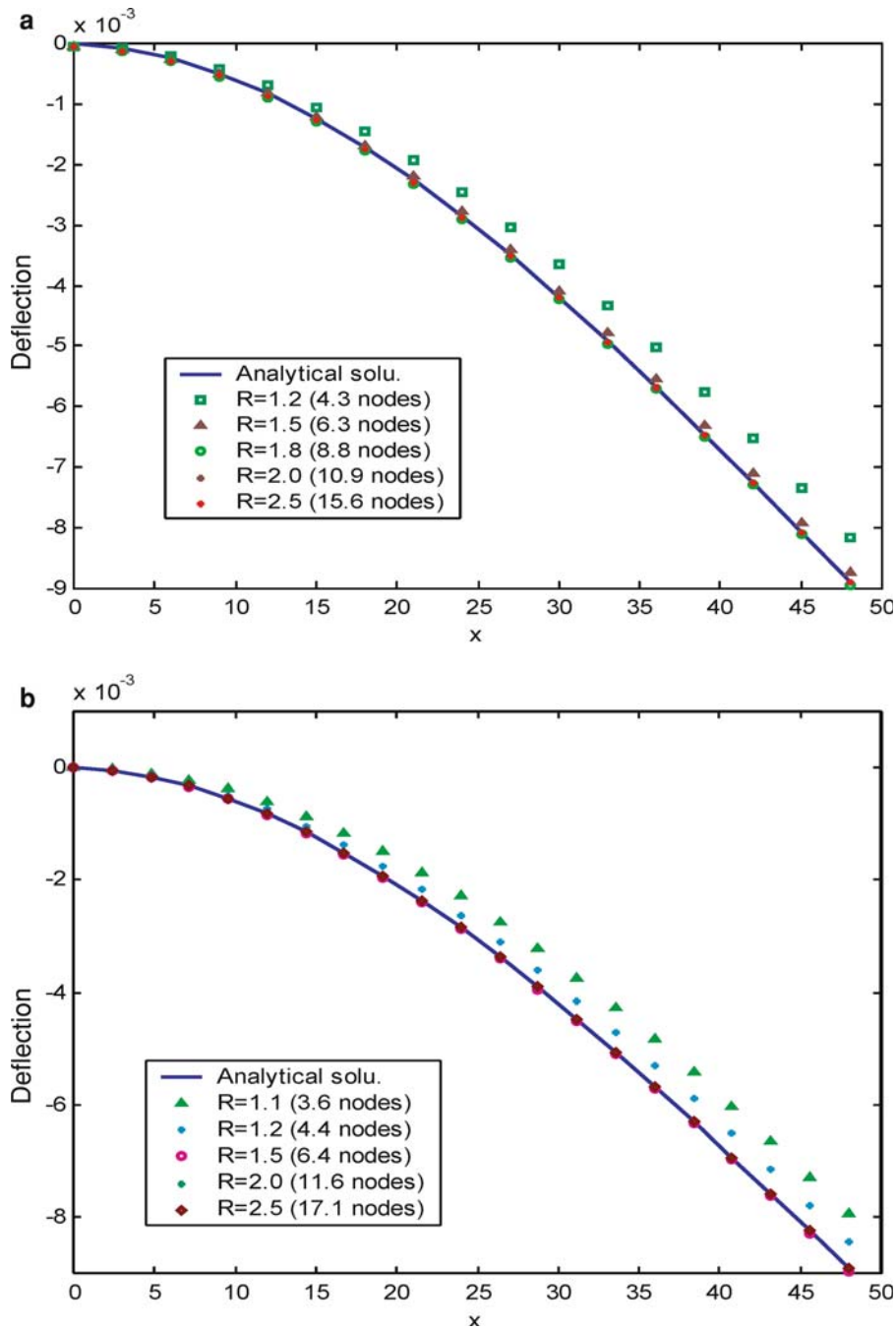


Fig. 5 Deflections of the cantilever beam using different sizes of support domain. ($q=1.01$, $n_p = 6$). (a) 17×5 nodes; (b) 21×9 nodes

$$u_i = \bar{u}_i \quad \text{on } \Gamma_u \tag{20}$$

where the superposed bar denotes the prescribed boundary displacements and n_i is the component of unit outward normal to the domain. Its variational weak form is expressed as

$$\int_{\Omega} \delta(\nabla_s \mathbf{u}) : \sigma d\Omega - \int_{\Omega} \delta \mathbf{u} \cdot \mathbf{b} d\Omega - \int_{\Gamma_f} \delta \mathbf{u} \cdot \bar{\mathbf{t}} d\Gamma = 0 \tag{21}$$

With the application of the derived MLM shape functions, the discretization of Eq. (21) yields (in matrix form)

$$\mathbf{Ku} = \mathbf{f} \tag{22}$$

3.1 Gauss quadrature (GI)

In order to evaluate the integrals in stiffness matrix, a background cell structure is required when using Gauss quadrature, which is independent of the field nodes (see Fig. 1).

Table 1 Errors of displacement using different sizes of support domain

R	1.2	1.5	1.8	2.0	2.5
a) 17×5 regular nodes					
Average supporting nodes	4.3	6.3	8.8	10.9	15.6
$e_d(\times 10^{-2})$ GI	16.57	3.95	1.59	0.425	0.180
NI	47.90	47.90	5.28	5.28	5.25
b) 21×9 regular nodes					
R	1.1	1.2	1.5	2.0	2.5
Average supporting nodes	3.6	4.4	6.4	11.6	17.1
$e_d(\times 10^{-2})$ GI	21.42	8.62	1.67	0.146	0.333
NI	11.77	11.77	11.77	1.42	1.42

The cell can be quadrilateral or triangular. For simplicity, quadrilateral cell structure is used in the paper. For uniformly distributed ($n_x \times n_y$) nodes, $(n_x - 1) \times (n_y - 1)$ rectangular cells are recommended with nodes located at grid points exactly. For irregularly scattered nodes, the numbers of cells in two directions are suggested as

$$n_x = \frac{l_x}{l_y} \sqrt{N}, \quad n_y = \frac{l_y}{l_x} \sqrt{N} \quad (23)$$

where l_x and l_y are maximum lengths of the domain in x - and y -direction and N the total node number in the domain.

Within each cell Gaussian quadrature method can be applied. The number of Gaussian points is determined by the node number in local support domain. The number of quadrature points depends on the number of nodes in a cell. The method used in EFG method is adopted here [12]

$$n_Q = \sqrt{m_c} + k \quad (24)$$

where ($n_Q \times n_Q$) quadrature points are used in each cell and m_c is the number of nodes in a cell. As the number of nodes covered in local support domain of MLM is normally less than that of EFG method, from our experience, $k=1$ is big enough for sufficient accuracy for general problems when (8–20) nodes are covered in support domain. However for problems with localized steep gradients (refer to the following heat conduction problem in Sect. 4), even higher order of quadrature such as $k=2$ is recommended.

3.2 Stabilized nodal integration (NI)

Based on the distribution of field nodes, the problem domain can be discretized using Voronoi diagram (see Fig. 2). To meet the linear exactness of Galerkin approximation, the following integration constraint should be satisfied [8, 4]

$$\int_{\Omega} \mathbf{B}_I^T(\mathbf{x}) d\Omega = \int_{\Gamma} \Phi_I^T(\mathbf{x}) d\Gamma \quad (25)$$

A smoothing operation is performed to the gradient of field function (displacement herein) in order to eliminate the error in the procedure of direct nodal integration, which is similar to the strain smoothing method used by [3]

$$\nabla u^h(\mathbf{x}_I) = \int_{\Omega} \nabla u^h(\mathbf{x}) \Phi(\mathbf{x} - \mathbf{x}_I) d\Omega \quad (26)$$

Integration by parts once leads to

$$\begin{aligned} \nabla u^h(\mathbf{x}_I) &= \int_{\Gamma} u^h(\mathbf{x}) \mathbf{n}(\mathbf{x}) \Phi(\mathbf{x} - \mathbf{x}_I) d\Gamma \\ &\quad - \int_{\Omega} u^h(\mathbf{x}) \nabla \Phi(\mathbf{x} - \mathbf{x}_I) d\Omega \end{aligned} \quad (27)$$

where Φ is a smoothing function and the weighted Shepard function is used as a distribution function, as given by

$$\Phi(\mathbf{x} - \mathbf{x}_I) = \frac{\phi(\mathbf{x} - \mathbf{x}_I)}{\sum_{J=1}^{n_I} \phi(\mathbf{x} - \mathbf{x}_J) A_J} \quad (28)$$

where $A_I = \int_{\Omega_I} d\Omega$ and Ω_I is the representative domain of node I (see Fig. 3). For simplicity, a piecewise constant function of ϕ is applied here, which is assumed to be unity within Ω_I and vanish somewhere else. So the above equation can be rewritten as

$$\Phi(\mathbf{x} - \mathbf{x}_I) = \begin{cases} 1/A_I & \mathbf{x} \in \Omega_I \\ 0 & \mathbf{x} \notin \Omega_I \end{cases} \quad (29)$$

Substituting of Φ into Eq. (27), one can get the smoothed gradient of displacement

$$\begin{aligned} \tilde{\nabla} u^h(\mathbf{x}_I) &= \int_{\Gamma_I} u^h(\mathbf{x}) \mathbf{n}(\mathbf{x}) \Phi(\mathbf{x} - \mathbf{x}_I) d\Gamma \\ &= \frac{1}{A_I} \int_{\Gamma_I} u^h(\mathbf{x}) \mathbf{n}(\mathbf{x}) d\Gamma \end{aligned} \quad (30)$$

where Γ_I is the boundary of the representative domain of node I . Similarly the smoothed strain can be obtained and given as

$$\tilde{\boldsymbol{\varepsilon}}^h(\mathbf{x}_I) = \sum_{J \in G_I} \tilde{\mathbf{B}}_J(\mathbf{x}_I) \mathbf{d}_J \quad (31)$$

where G_I is a set of nodes in the influence domain of node I or those whose shape function supports cover node I . For 2-D case

$$\begin{aligned} \tilde{\mathbf{B}}_J(\mathbf{x}_I) &= \begin{bmatrix} \tilde{b}_{J1}(\mathbf{x}_I) & 0 \\ 0 & \tilde{b}_{J2}(\mathbf{x}_I) \\ \tilde{b}_{J2}(\mathbf{x}_I) & \tilde{b}_{J1}(\mathbf{x}_I) \end{bmatrix}, \quad \tilde{b}_{Jk}(\mathbf{x}_I) \\ &= \frac{1}{A_I} \int_{\Gamma_I} \Psi_J(\mathbf{x}) n_k(\mathbf{x}) d\Gamma, \quad (k = 1, 2) \end{aligned} \quad (32)$$

If a two-point trapezoidal rule is used for integration along each segment of boundary Γ_I^l of Ω_I , the above equation can be transformed to its algebraic form

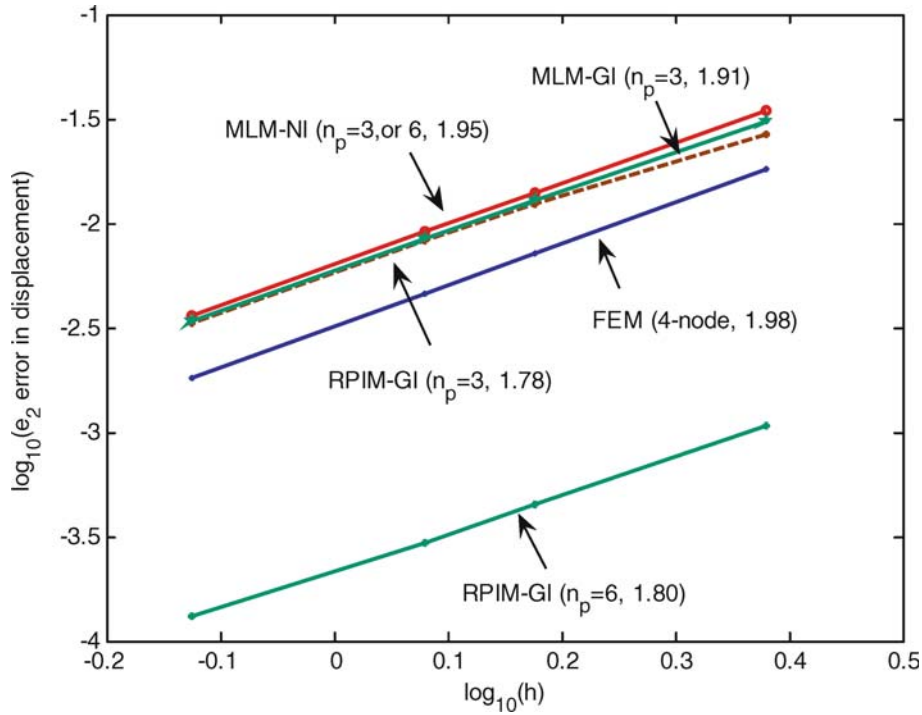


Fig. 6 Comparison of convergence rate in displacement norm among FEM, MLM and RPIM

$$\tilde{b}_{Jk}(\mathbf{x}_I) = \sum_{i=1}^M \left[\Psi_J(\mathbf{x}_i) n_{ik}^I \frac{l_i^I}{2} + \Psi_J(\mathbf{x}_j) n_{ik}^I \frac{l_i^I}{2} \right] \quad (33)$$

where i and j ($= i+1$) are two end points of boundary segment of Γ_i^I , whose length and outward unit normal are l_i^I and n_i^I , respectively. Similarly, Gauss integration can also be employed for the boundary integration along each segment. It can totally eliminate zero-energy mode appearing in some special cases [19].

It has been proved that the strain smoothing stabilization can exactly satisfy the integration constraint of Eq. (25) [4].

The numerical procedure for NI using two-point trapezoidal rule is briefed as follows.

- (1) Form Voronoi diagram for given field nodes and gather nodal information;
- (2) Generate MLM shape functions and record corresponding supporting nodes at each vertex point;
- (3) Loop over all the field nodes:
 - a. Determine the area and outward unit normal of each side for sub-domain Ω_I ;
 - b. Compute the \mathbf{B} matrix using Eq. (33);
 - c. Evaluate the stiffness matrix;
 - d. Assemble the contribution of the current node to form system matrices and vectors.
- (4) Form external loading vector and implement essential boundary conditions;
- (5) Solve the system equations to obtain the nodal displacements;
- (6) Evaluate strains and stresses at each node.

4 Numerical examples

4.1 Cantilever beam

A cantilever beam with length L and height D is studied here. It is subjected to a parabolic traction at the free end as shown in Fig. 1. The beam is assumed to have a unit thickness so that plane stress theory is valid here. The analytical solution is available and can be found in a textbook by Timoshenko and Goodier [16].

$$u_x = \frac{Py}{6EI} \left[(6L - 3x)x + (2 + \nu)(y^2 - \frac{D^2}{4}) \right]$$

$$u_y = -\frac{P}{6EI} \left[3\nu y^2(L - x) + (4 + 5\nu)\frac{D^2x}{4} + (3L - x)x^2 \right] \quad (34)$$

where the moment of inertia I of the beam is given by

$$I = D^3/12 \quad (35)$$

The stresses corresponds to the displacements Eq. (34) are

$$\sigma_x(x, y) = \frac{P(L - x)y}{I}$$

$$\sigma_y(x, y) = 0$$

$$\sigma_{xy}(x, y) = -\frac{P}{2I} \left(\frac{D^2}{4} - y^2 \right) \quad (36)$$

The related parameters are taken as $E=3.0 \times 10^7 \text{ kPa}$, $\nu = 0.3$, $D = 12 \text{ m}$, $L = 48 \text{ m}$ and $P = 1000 \text{ N}$.

In order to study the convergence rates of the three point interpolation methods, two norms are defined here, i.e., displacement norm and energy norm. The displacement norm

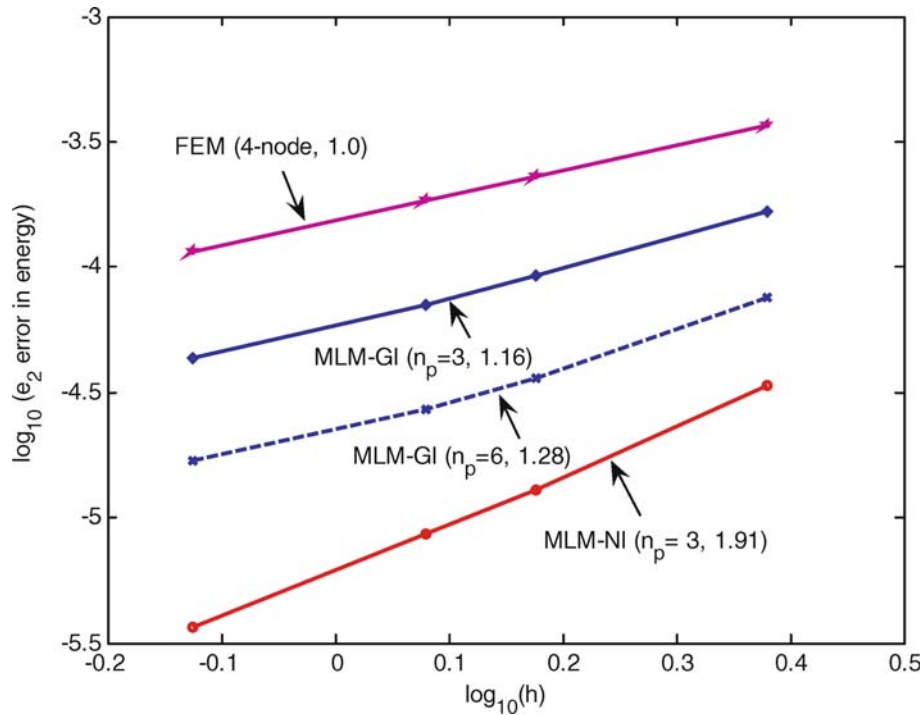


Fig. 7 Comparison of convergence rate in energy norm between FEM and MLM

Table 2 Errors of displacement and energy using different nodal densities (MLM-GI) ($R=2.0$, $q=1.01$)

Node distribution	Average supporting node	$n_p = 6$		$n_p = 3$	
		e_e	e_d	e_e	e_d
11×5	10.8	1.45e-4	7.38e-3	2.95e-4	3.78e-2
21×6	11.2	7.49e-5	2.70e-3	1.66e-4	3.09e-2
33×9	11.7	3.63e-5	1.16e-3	9.18e-5	1.30e-2
41×11	11.8	2.70e-5	8.70e-4	7.11e-5	8.39e-3
65×17	12.1	1.68e-5	5.71e-4	4.30e-5	3.36e-3

Table 3 Comparison of computational time between MLM and RPIM ($R=2.0$, $q=1.01$)

Node distribution	MLM (sec)			RPIM (sec)	
	$n_p = 3$ (NI)	$n_p = 3$ (GI)	$n_p = 6$ (GI)	$n_p = 3$ (GI)	$n_p = 6$ (GI)
11×5	1.08	6.33	6.45	4.74	6.38
21×6	2.13	18.38	13.61	18.94	19.77
33×9	10.31	82.02	82.86	74.18	74.74
41×11	19.97	186.13	196.39	180.09	193.78
65×17	185.58	1587.3	1597	—	—

uses the relatively errors of displacement at all nodes as follows

$$e_d = \frac{\sum_{i=1}^N |u_i^{Numer} - u_i^{Exact}|}{\sum_{i=1}^N |u_i^{Exact}|} \quad (37)$$

and the energy norm is defined by

$$e_e = \frac{1}{2LD} \left[\int_{\Omega} (\varepsilon^{Numer} - \varepsilon^{Exact})^T \mathbf{D} (\varepsilon^{Numer} - \varepsilon^{Exact}) \right]^{1/2} \quad (38)$$

4.1.1 Effect of shape parameters

Two commonly used RBFs are listed below for 2-D case, i.e., Multiquadrics and Gaussian RBFs.

$$r(\mathbf{x}_i) = [(x - x_i)^2 + (y - y_i)^2 + Cd_c^2]^q \text{ (MQ-RBF)} \quad (39)$$

$$r(\mathbf{x}_i) = \exp[-\alpha((x - x_i)^2 + (y - y_i)^2)/d_c^2] \text{ (EXP-RBF)} \quad (40)$$

where d_c is a characteristic length or average nodal spacing. Two shape parameters (C and q) appear in MQ-RBF and one (α) in EXP-RBF, which have great effect on the accuracy of final results [18]. In this paper only MQ-RBF is explored.

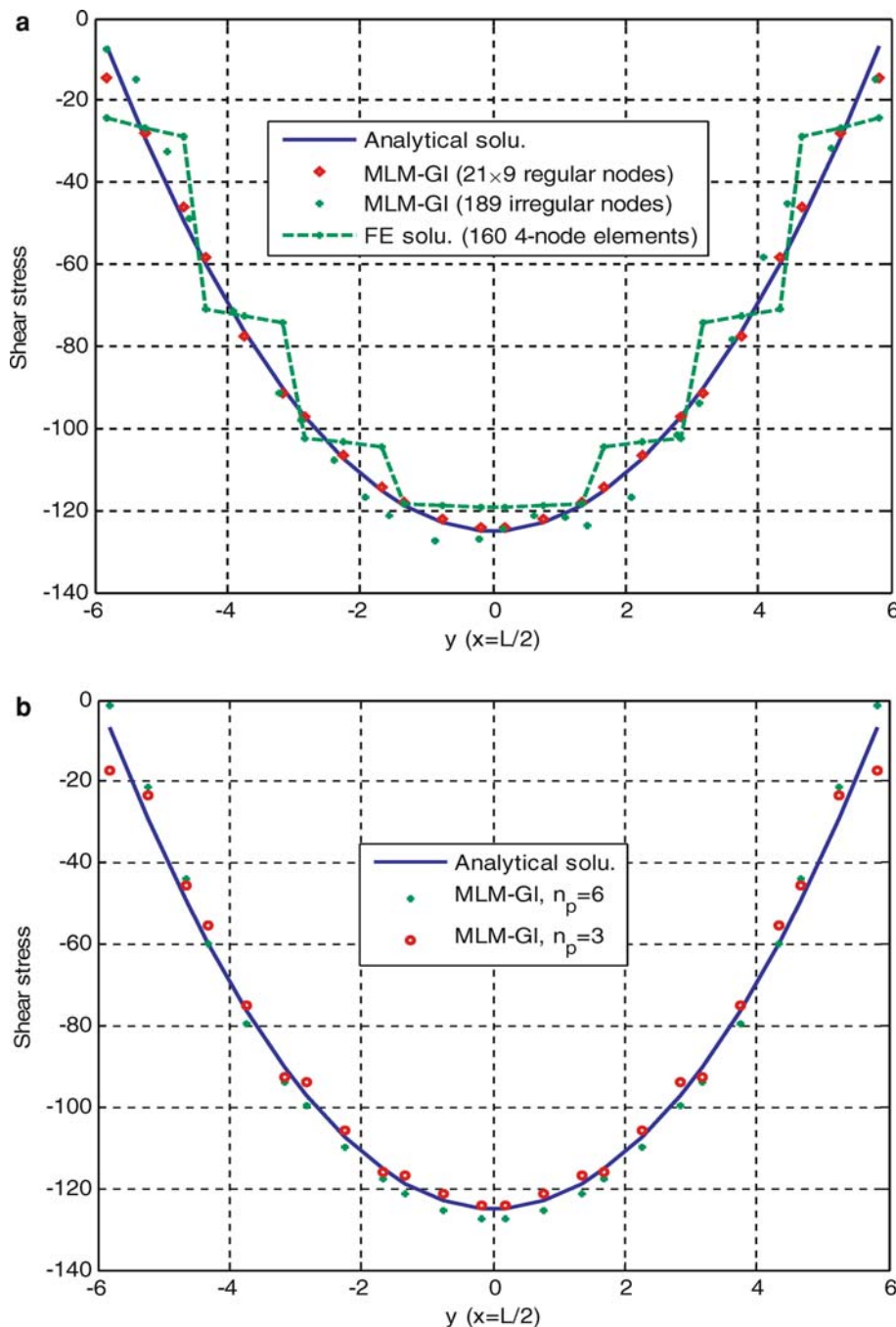


Fig. 8 Shear stress on $x=L/2$ using 21×9 regular nodes using (a) using FEM and MLM-GI ($R=3.0$); (b) using different polynomial terms of MLM-GI ($R=2.0$) and (c) MLM-NI

Through numerical testing, it is found that parameter C has insignificant effect on final results. So we fix $C=0$ in the following examples. The new form of MQ is termed accordingly as modified MQ-RBF.

The effect of q is quite different from that in data or curve fitting. In the weak-form formulation, local compact support domain is used to produce banded system equations. Theoretical explanation of the effect of parameter q is very difficult and numerical experiment is often used. 21×9 regularly

distributed nodes are used to discretize the cantilever beam. 20×8 rectangular background cells are used for Gauss integration and 3×3 quadrature order is applied in each cell. The value of q is varied from 0.95 to 1.05 and note that 1.0 is never used since otherwise the MQ-RBF will degenerate into polynomials. The errors in both displacement norm and energy norm are demonstrated in Fig. 4. It is noticed that, when q is close to 1.0, more accurate results are obtained. Hence, if not specified otherwise, $q = 1.01$ is used in the following

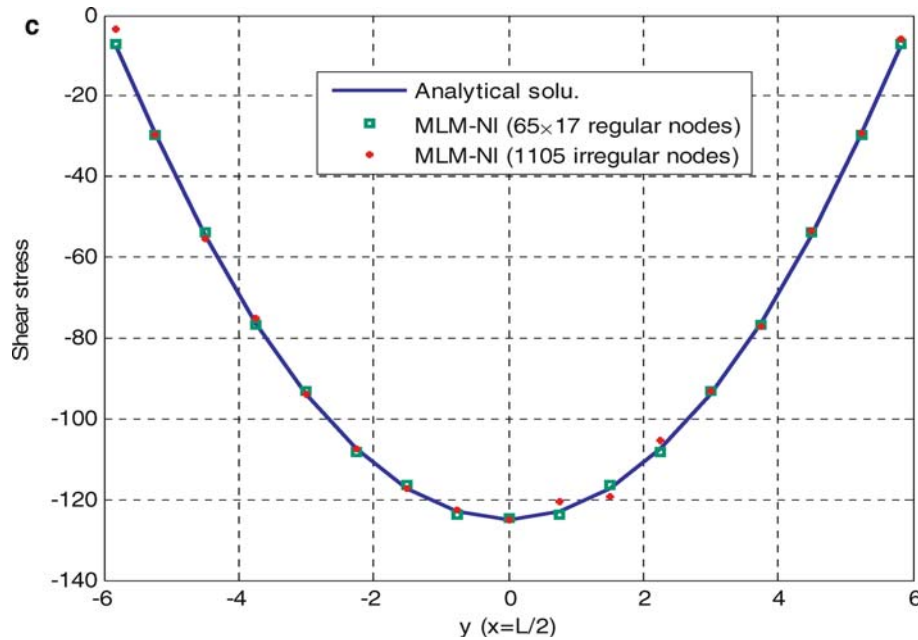


Fig. 8 (contd.)

examples. Comparing the Gauss integration and nodal integration, it can be seen that shape parameter is less sensitive to the final results in the latter scheme.

4.1.2 Size of support domain

The size of support domain, or the number of nodes covered in support domain, also plays an important role on accuracy of final results. If too small number of nodes is included, one may fail to get accurate results even though the problem domain is discretized by suitable number of nodes. Support domain can be a rectangle, a circle or an ellipse for uniform nodal arrangement. An ellipse is used in this study as the nodal spacing may be different in two directions (see Fig. 1). The relationship can be defined as

$$\frac{(x_q - x_i)^2}{a^2} + \frac{(y_q - y_i)^2}{b^2} < R^2 \quad (41)$$

where R is termed as axial parameter; (a, b) are nodal spacings in two directions. (x_q, y_q) and (x_i, y_i) correspond to quadrature point and field node, respectively. (17×5) and (21×9) regularly spaced nodes are taken for instance to examine the size of support domain. The centerline deflection of the beam is plotted in Fig. 5 when parameter R increases from 1.1 to 2.5. Some of the results are also listed in Table 1. It can be seen that, when supporting nodes are less than 6 using GI, the results are not accurate. Generally, the larger the number of nodes covered in support domain, the more accurate the solutions. Normally, 6–20 supporting nodes are sufficient to give good solutions. By comparison, when R is larger than a certain value in NI, e.g. $R=1.8$ for 17×5 nodes, the error of displacement is almost constant. To enhance the accuracy, one can increase the number of field nodes. Accordingly,

$R = 2.0$ – 3.0 is often used in the study. For irregular nodal distribution, a circular support domain may be employed with radius

$$r_s = R d_c \quad (42)$$

where d_c is a characteristic length that relates to the nodal spacing near the point in consideration. For 2-D case, it is defined as

$$d_c = \frac{\sqrt{A_s}}{\sqrt{n_s - 1}} \quad (43)$$

where A_s is an estimated area that is covered by the support domain and n_s the number of nodes enclosed in the support domain ranging from 10 to 30. Similarly, $R = 2.0$ – 3.0 leads to good results.

4.1.3 Comparison of convergence rate and efficiency among FEM, MLM and RPIM

Four regular nodal patterns are employed to examine the convergence rate of the three methods, i.e., 21×6 , 33×9 , 41×11 , 65×17 evenly spaced nodes. Linear and quadratic polynomials ($n_p = 3, 6$) are included respectively in the interpolation bases for MLM and RPIM. For comparison, four-node finite elements with identical node densities are also used for the analysis. RPIM uses the same nodal density, support domain size and shape parameters as the MLM. The convergence rates in displacement norm and energy norm are shown in Figs. 6 and 7, respectively. The quantity h is equivalent to the maximum mesh size in the FEM. It is observed that the MLM-GI achieves a slightly higher convergence rate in energy norm but generally the same in displacement norm when compared to the FEM. When comparing MLM-GI and

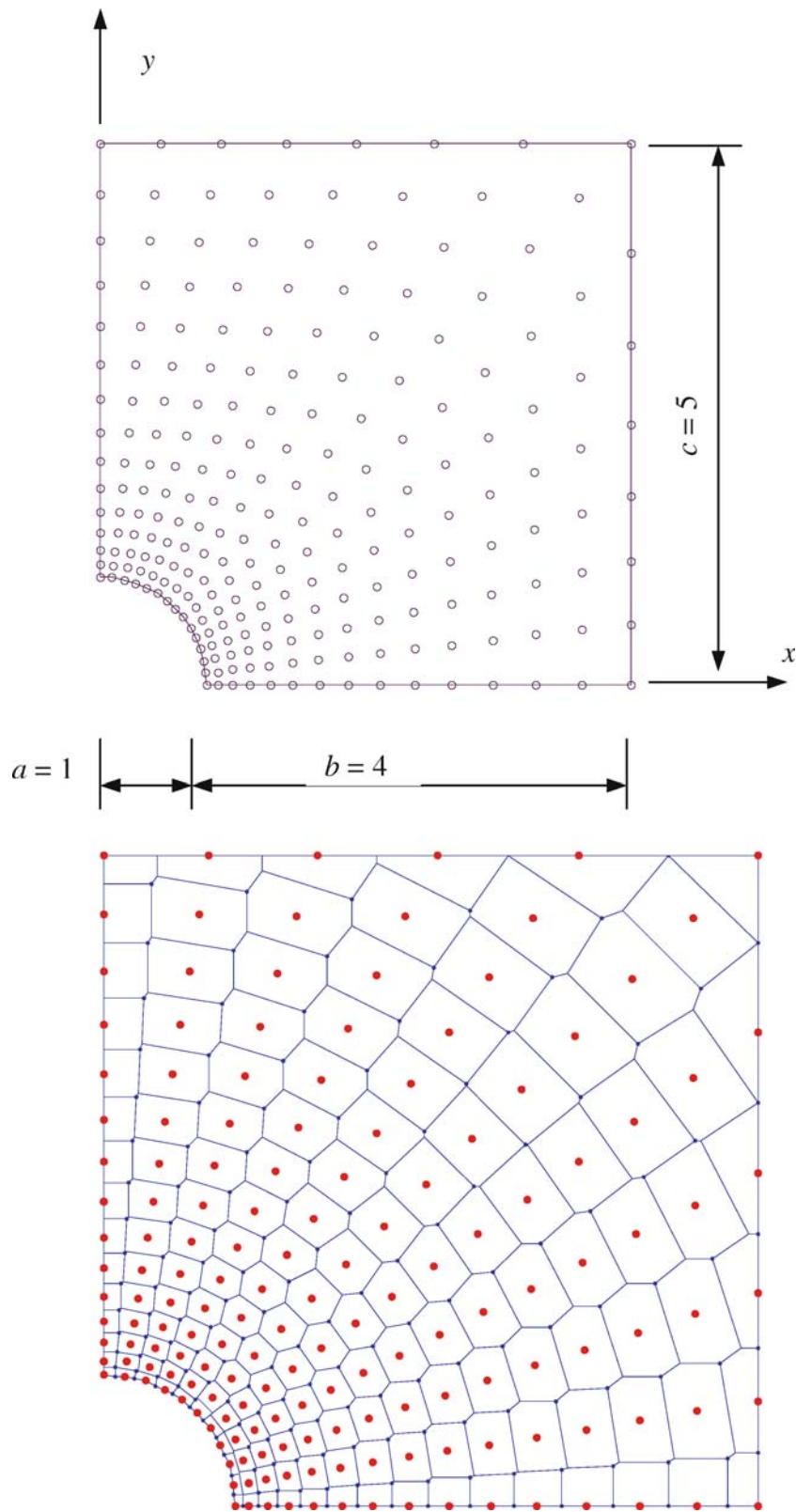


Fig. 9 Nodal distribution in a plate with a central hole and its Voronoi diagram

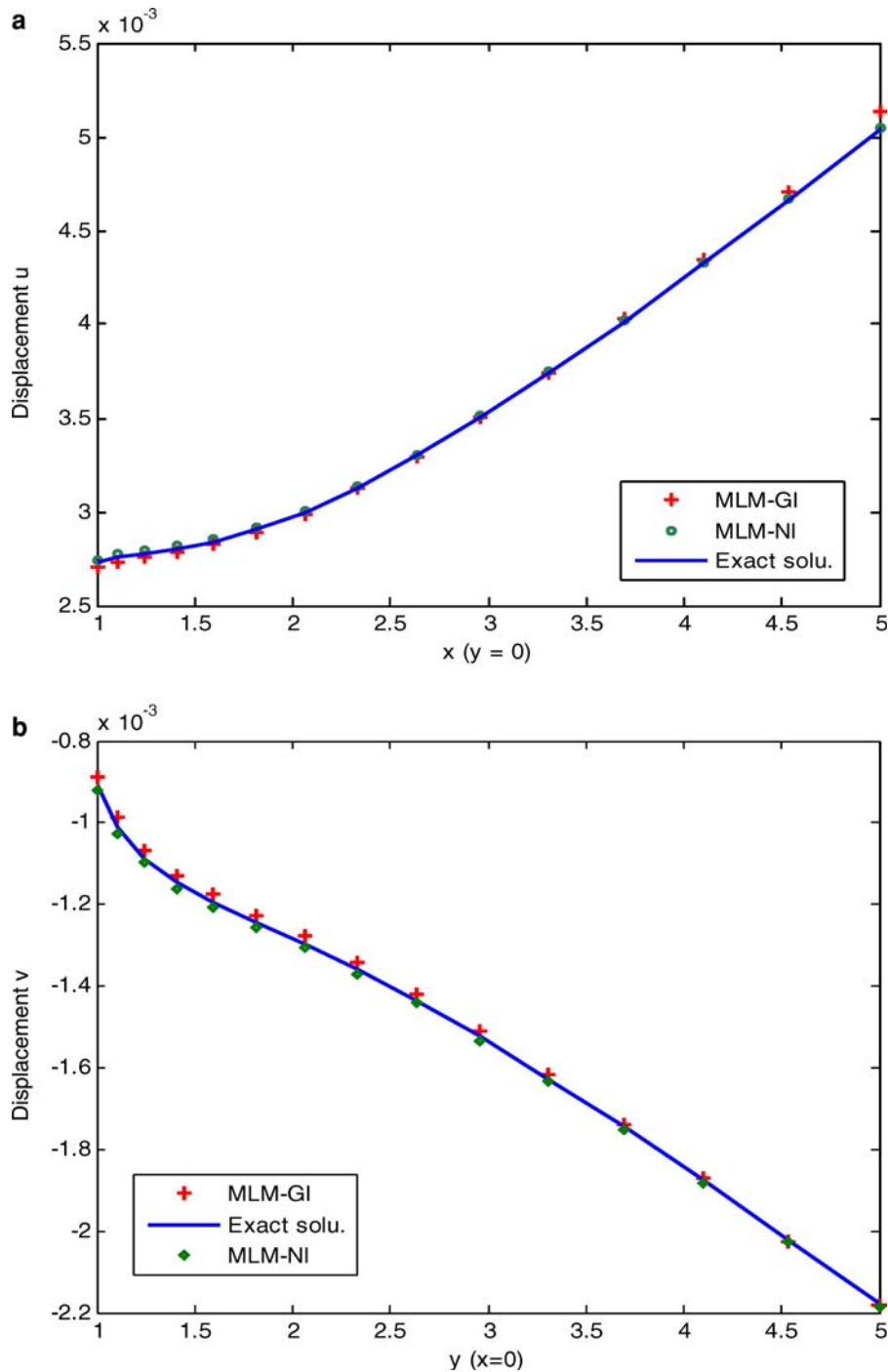


Fig. 10 Results of an infinite plate with a central hole subjected a unidirectional tensile load. (a) Displacement u on $y=0$; (b) Displacement v on $x=0$ and (c) Stress σ_x on $x=0$

RPIM-GI, one can see that both methods achieve nearly same rate whereas the latter is of higher accuracy of displacement than the former when $n_p = 6$. Their convergence rates in energy norm are almost equivalent. Quadratic polynomials give better results than linear ones while both of them are more accurate than those obtained by FEM. It is observed that MLM-NI achieves much higher convergence rate and accuracy in energy than both MLM-GI and RPIM-GI as well as

4-node FEM. Examining the errors listed in Table 2, one can see that the results of MLM-GI using linear polynomials in displacement norm are one order larger than using quadratic polynomials, whereas the latter do not entail great computational costs additionally. For MLM-NI, the added linear and quadratic polynomials give comparably accuracy in both displacement and energy. Hence only linear polynomials are used in MLM-NI if not stated otherwise. The simulation time

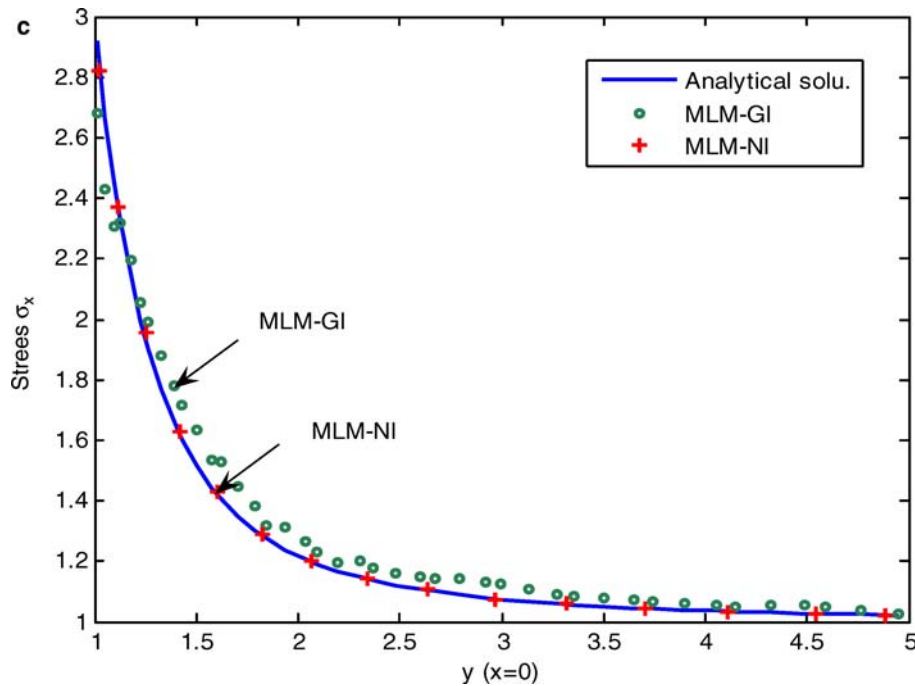


Fig. 10 (contd.)

given in Table 3 shows that the computational cost for both MLM-GI and RPIM-GI are nearly the same, which testify the correctness of Eq. (17). In addition, quadratic polynomials included do not increase the cost greatly. On account of this, quadratic polynomials are recommended in interpolation bases in MLM-GI. When comparing GI and NI, it is found that NI can significantly reduce the computational time especially for larger number of field nodes used.

It should be mentioned that when node number covered in support domain is less than the polynomials used in interpolation basis, i.e., $n < n_p$ PRIM fails to work due to the singularity of moment matrix whereas MLM can still work properly. This is one advantage of MLM over RPIM.

From the formulation of MLM, it is seen that the construction of shape function in this method is more complicated than 4-node finite elements, which is different from point to point due to locally changing node pattern and can, in consequence, only be evaluated in the process of simulation. Local interpolation uses more nodes than FEM. The higher order of approximation accordingly requires more quadrature points in one integration cell. Therefore the CPU time required for MLM is approximately three to six times more than 4-node FEM.

4.1.4 Regular/Irregular nodal pattern

To investigate the effect of the nodal distribution, 21×9 regular nodes and 189 irregular nodes are used as shown in Fig. 1. Figure 8 illustrates the comparison of the shear stress computed analytically and using the present method on the section $x = L/2$. For comparison, 20×8 four-node finite elements are also used for the same problem. Only stresses at Gauss

points are averaged and plotted for simplicity in MLM-GI. In MLM-NI, the calculated stresses are assumed to belong to the central point in the representative domain of boundary nodes. Very good agreement is observed for both regular and irregular nodal distribution in the application of MLM. Comparing the effect of the number of polynomial terms on the stress distribution in MLM-GI, one can see quadratic polynomials enhance the accuracy. The present results are almost continuous and post-processing of stresses is not required.

4.2 Infinite plate with a hole

Figure 9 represents a plate with a central circular hole subject to a unidirectional tensile load of $1.0 N/m$ at infinity in the x -direction and Fig. 9b gives the Voronoi diagram in NI. Due to its symmetry, only the upper right quadrant of the plate is modeled. Plane strain condition is considered, and $E=1.0 \times 10^3 N/m^2$, $\nu = 0.3$. Symmetry conditions are imposed on the left and bottom edges, and the inner boundary of the hole is traction free. The exact solution for the stresses is [16]

$$\begin{aligned}
 \sigma_x(x, y) &= 1 - \frac{a^2}{r^2} \left[\frac{3}{2} \cos 2\theta + \cos 4\theta \right] + \frac{3a^4}{2r^4} \cos 4\theta \\
 \sigma_y(x, y) &= -\frac{a^2}{r^2} \left[\frac{1}{2} \cos 2\theta - \cos 4\theta \right] - \frac{3a^4}{2r^4} \cos 4\theta \\
 \sigma_{xy}(x, y) &= -\frac{a^2}{r^2} \left[\frac{1}{2} \sin 2\theta + \sin 4\theta \right] + \frac{3a^4}{2r^4} \sin 4\theta \quad (44)
 \end{aligned}$$

where (r, θ) are the polar coordinates and θ is measured counterclockwise from the positive x -axis. Traction boundary con-

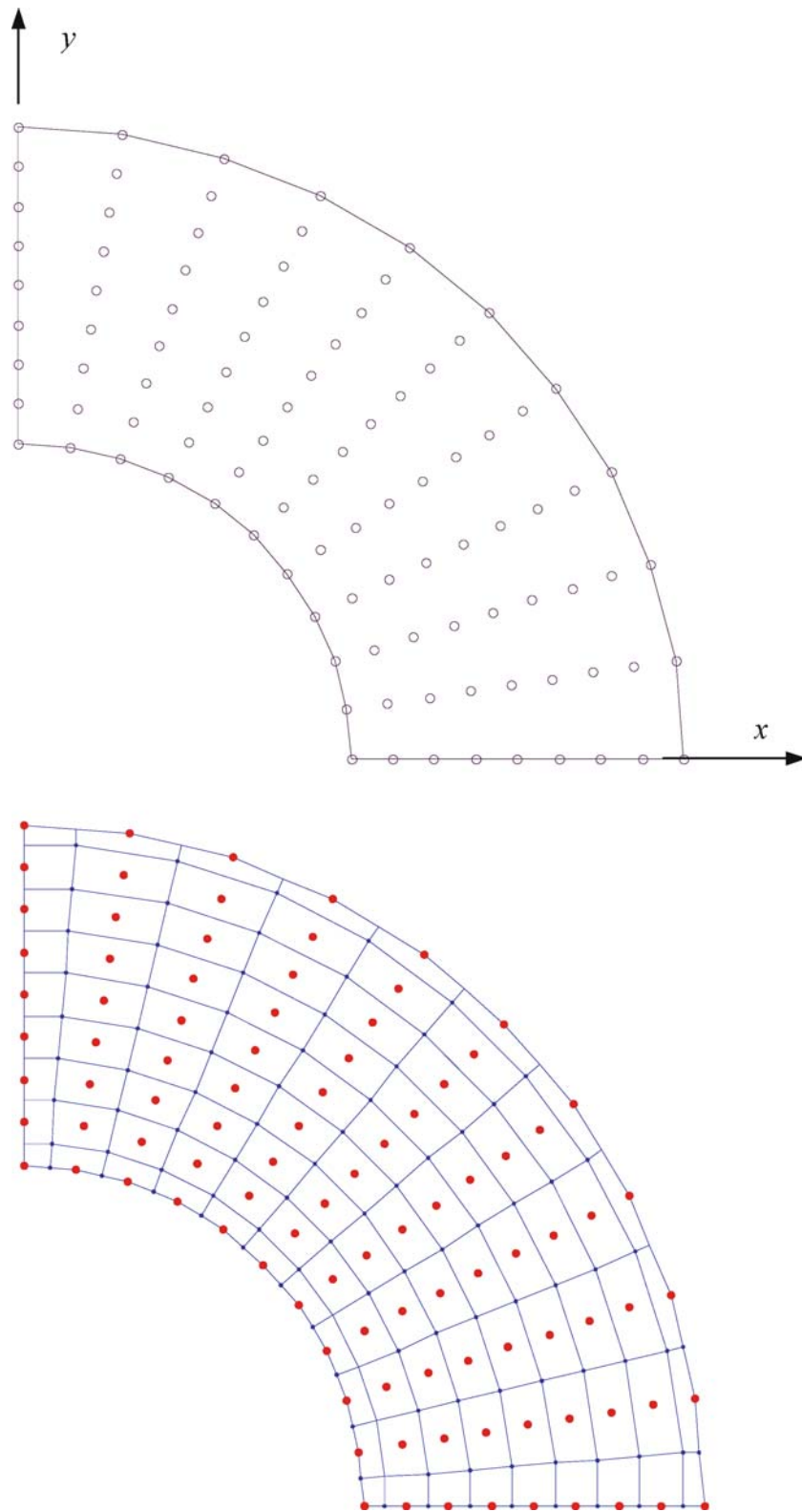


Fig. 11 Nodal arrangement for a pressured cylinder and its Voronoi diagram

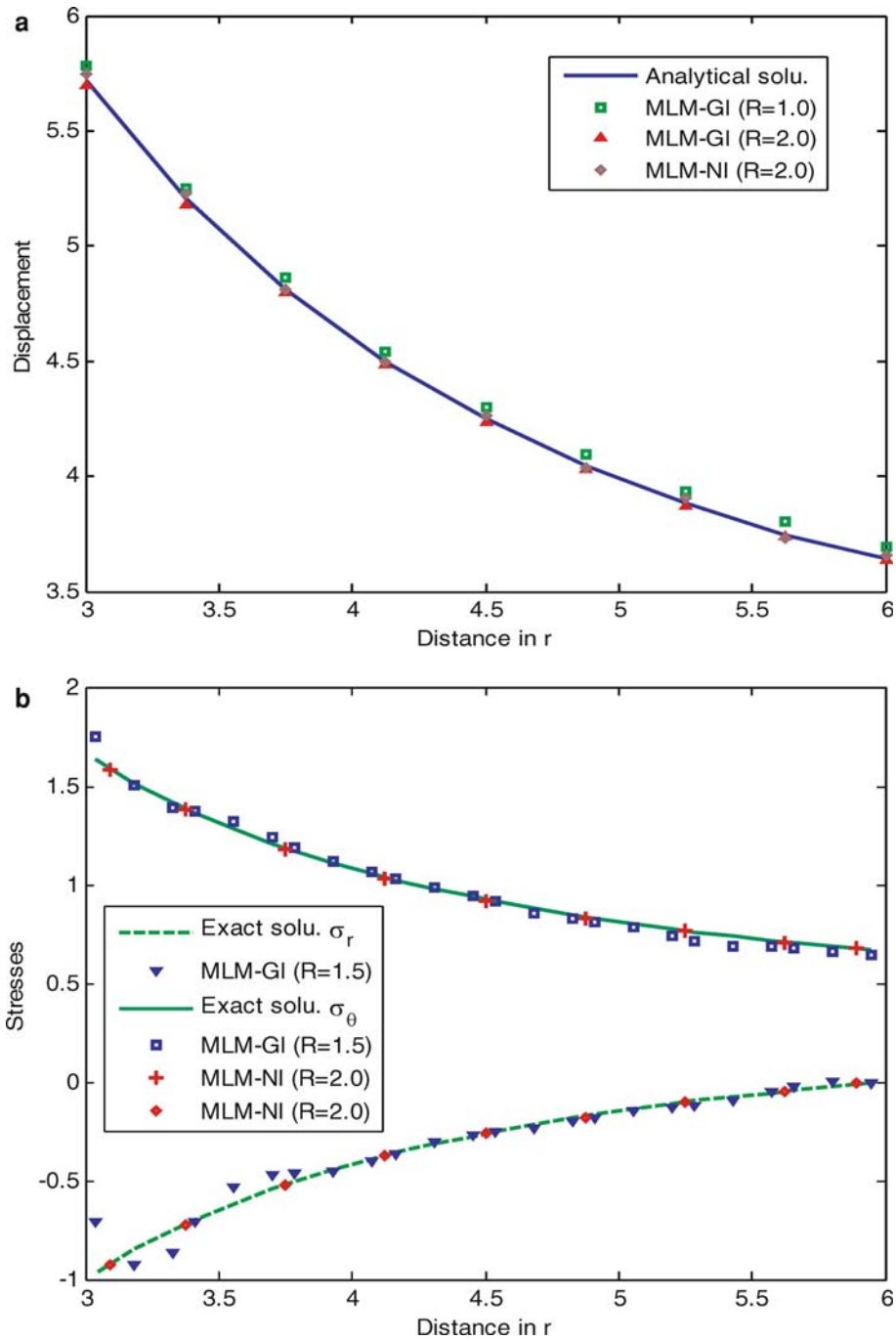


Fig. 12 (a) Displacement u_r and (b) stresses in the pressured cylinder

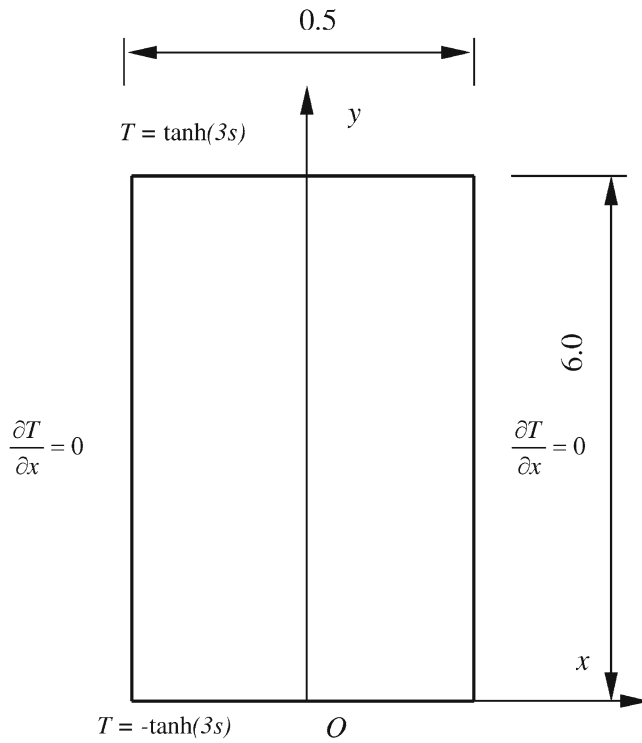
ditions are imposed on the right ($x=5$) and top ($y=5$) edges based on the exact solution Eq. (44).

The domain is discretized by 225 nodes and 194 sectorial background cells are used for Gauss integration. A circular support domain is used for simplicity. Due to the changing nodal densities in problem domain, a subroutine is developed to automatically vary the radius of support domain such that the number of selected nodes ranges between 12 and 30 in GI. The displacement u_r along $y=0$ and the stress σ_x along $x=0$ using the present method are plotted in Fig. 10. It can be

seen that the present results coincide well with the analytical ones. Comparing the GI and NI schemes, one can see that NI generates more accurate and stable results especially for stress analysis.

4.3 Pressured thick-walled cylinder

A thick-walled cylinder of internal radius R_1 and outer radius R_2 is analyzed here, which is subjected to internal pressure P . The outer edge is traction-free. The cylinder is assumed to be



Heat source: $b(x, y) = 2s^2 \sec h^2[s(y-3)] \tanh[s(y-3)]$

Fig. 13 A heat conduction problem in a rectangular plate

sufficiently long so that plane strain condition is applicable. The numerical values used are $R_1 = 3$, $R_2 = 6$, $P = 1.0$ with material properties $E = 1.0$ and $\nu = 0.3$. The plane strain Lamé solution can be written as [16]

$$\begin{aligned} u_r &= C_1 r + \frac{C_2}{r} \\ \sigma_{rr} &= C_3 - \frac{C_4}{r^2} \\ \sigma_{\theta\theta} &= C_3 + \frac{C_4}{r^2} \end{aligned} \quad (45)$$

where the constants C_1 to C_4 depend on the geometry and boundary conditions. In this problem, they take the values: $C_1 = 0.1733$, $C_2 = 15.6$, $C_3 = 0.3333$ and $C_4 = 12.0$. Due to the symmetry, only one quarter of the cross section is considered and modeled by 99 nodes, as shown in Fig. 11. A circular support domain is employed with radius $R = 1.0$ and $R = 1.5$ respectively. The computed displacements and stresses are plotted in Fig. 12. It can be seen that both the displacements and the stresses obtained by the present method in very good agreement with analytical ones. For displacement of MLM-GI, when R increases from 1.0 to 1.5, the present results approach analytical ones. It is noticed that the results of MLM-GI clearly deviate from the exact ones for points near inner surface. This may be caused by the reason that insufficient nodes are covered in support domain for quadrature points in the region. Once again the MLM-NI yields much better stresses than MLM-GI even near boundaries.

4.4 High-gradient heat conduction problem

A heat conduction problem is considered here in a rectangular plate (as shown in Fig. 13) with heat source

$$b(x, y) = 2s^2 \sec h^2[s(y-3)] \tanh[s(y-3)] \quad (46)$$

The boundary conditions are given by

$$T = -\tanh(3s) \quad \text{at } y = 0$$

$$T = \tanh(3s) \quad \text{at } y = 6 \quad (47)$$

$$\frac{\partial T}{\partial x} = 0 \quad \text{at } x = -0.25 \text{ and } x = 0.25$$

The exact solution of this problem is

$$T = \tanh[s(y-3)] \quad (48)$$

As shown in the study by Belytschko et al. [2] this problem has a very high gradient of temperature near $y = 3.0$. In Eq. (46), the quantity s is a free parameter. The bigger the value of s , the higher the gradient of field T . As the steep gradient occurs only near the area $2.5 \leq y \leq 3.5$. A very dense nodal pattern with (10×40) even nodes is used to discretize this area. For the other two areas, (10×25) regularly distributed nodes are used, respectively. For comparison, once again the four-node finite elements with the same nodal distribution are applied to analyze this problem. Note that $s = 40$ is used in the analysis. In the MLM-GI, linear polynomials are included for interpolation basis. An elliptical support domain with $R = 2.0$ is used as defined in Eq. (41). Due to the high gradient of field in consideration, (4×4) Gauss quadrature order is used in both methods.

Figure 14 illustrates the comparison of temperature between the exact solution and the numerical solution obtained by MLM-GI. It is observed that very good agreement is achieved. The computed gradient T_y by the MLM as shown in Fig. 15 are much better than those by FEM, especially for larger s . It should be mentioned that, as only the gradient values at the quadrature points are plotted for simplicity without curve fitting, this is responsible for the phenomenon that the numerical value at the tip is smaller than the exact one.

5 Conclusions

In this work a mesh-free minimum-length method (MLM) is proposed for solving 2-D solids and heat conduction problems. This method employs polynomial terms as well as modified radial basis functions (RBFs) to interpolate field variables using arbitrary nodal distribution. Minimum length procedure is used to construct a functional from which the shape functions are derived. Weak form integration is numerically conducted using Gauss integration and nodal integration. Some numerical examples are studied and related parameters are also examined. From the research the following conclusions can be drawn.

- (1) Due to the delta function property of the derived shape functions, the essential boundary conditions can be enforced conveniently as in conventional FEM. In MLM-GI, quadratic polynomials can improve the accuracy by

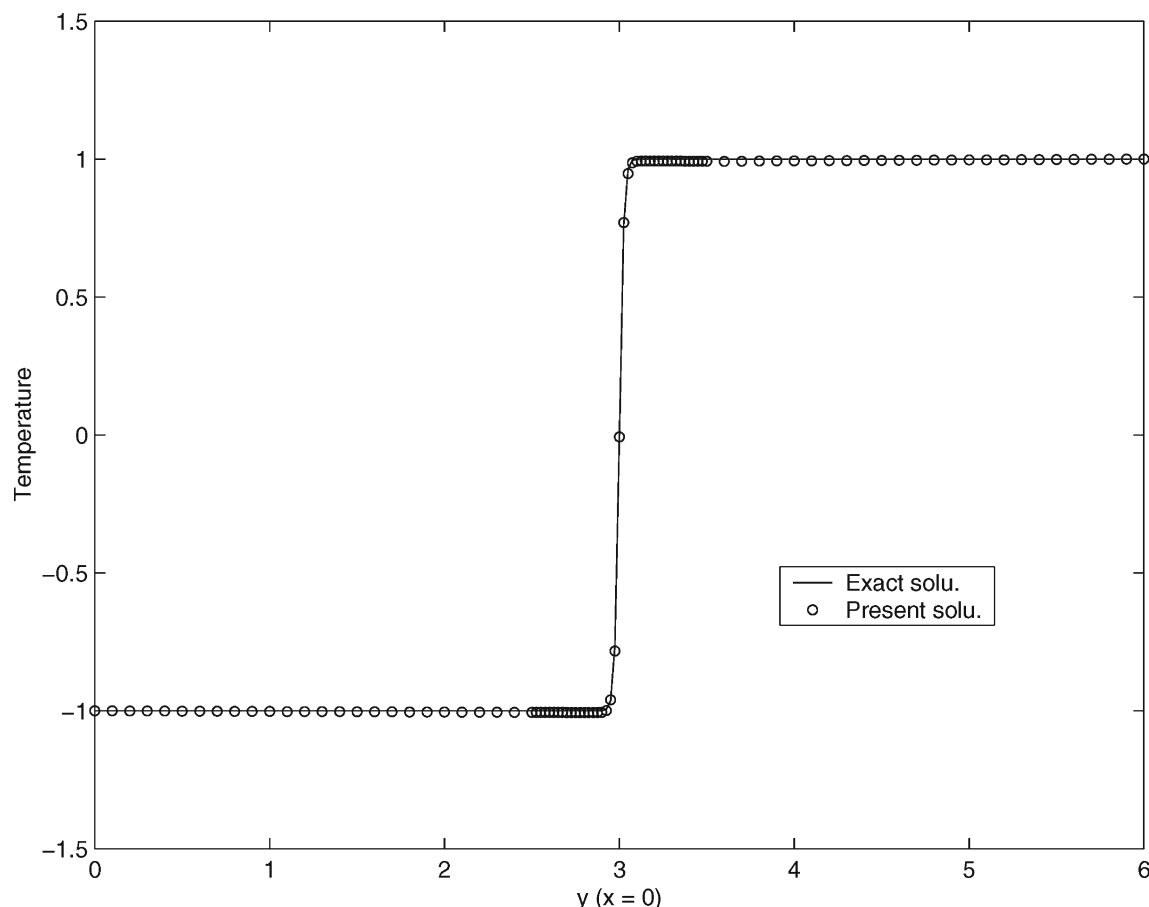


Fig. 14 Comparison of temperature between exact solution and MLM-GI results for the high-gradient problem

one order for energy when compared with linear polynomials.

- (2) In the modified MQ-RBFs, the shape parameter q around 1.0 ($0.98 < q < 1.03$; $q \neq 1.0$) is recommended for good resolution of final results. MLM is not sensitive to the shape parameter C in the conventional MQ-RBF and thus removed from its original form. The selection of shape parameters is no longer required to consider in the present method.
- (3) Stabilized nodal integration is used for weak-form integration. It is found that nodal integration can significantly improve the accuracy and stability and computational time is greatly reduced as compared to Gauss integration. As the representative domain for each node is established uniquely using Voronoi diagram, no additional background structure is required over the entire problem domain.
- (4) The method shows higher accuracy than the four-node finite elements especially for problems with localized steep gradients while its convergence rate is also comparable with that of FEM. Good results can be obtained for both primary and secondary field variables.
- (5) Local support domain can be circular, elliptical or rectangular. For elliptical support domain, the axial parameter

can be chosen as $2.0 < R < 3.0$ such that 10–20 nodes are covered in sub-domain. Irregularly distributed nodal distribution performs well and it does not degrade prominently the accuracy of final results. No singularity occurs for moment matrix in numerical analysis.

In conclusion, MLM achieves equivalent accuracy and convergence rate as compared to RPIM. It can serve as a substitute for RPIM to obtain shape function with delta property. MLM-NI shows better performance in terms of accuracy and efficiency than MLM-GI.

References

1. Atluri SN, Zhu T (1998) A new meshless local Petrov-Galerkin (MLPG) approach in computational mechanics. *Comput Mech* 22:117–127
2. Belytschko T, Lu YY, Gu L (1994) Element-free Galerkin methods. *Int J Numer Meth Eng* 37:229–256
3. Chen JS, Wu CT, Belytschko T (2000) Regularization of material instabilities by meshfree approximations with intrinsic length scales. *Int J Numer Meth Engng* 47:1303–1322
4. Chen JS, Wu CT, Yoon S, You Y (2001) A stabilized conforming nodal integration for Galerkin meshfree method. *Int J Numer Meth Eng* 50:435–466

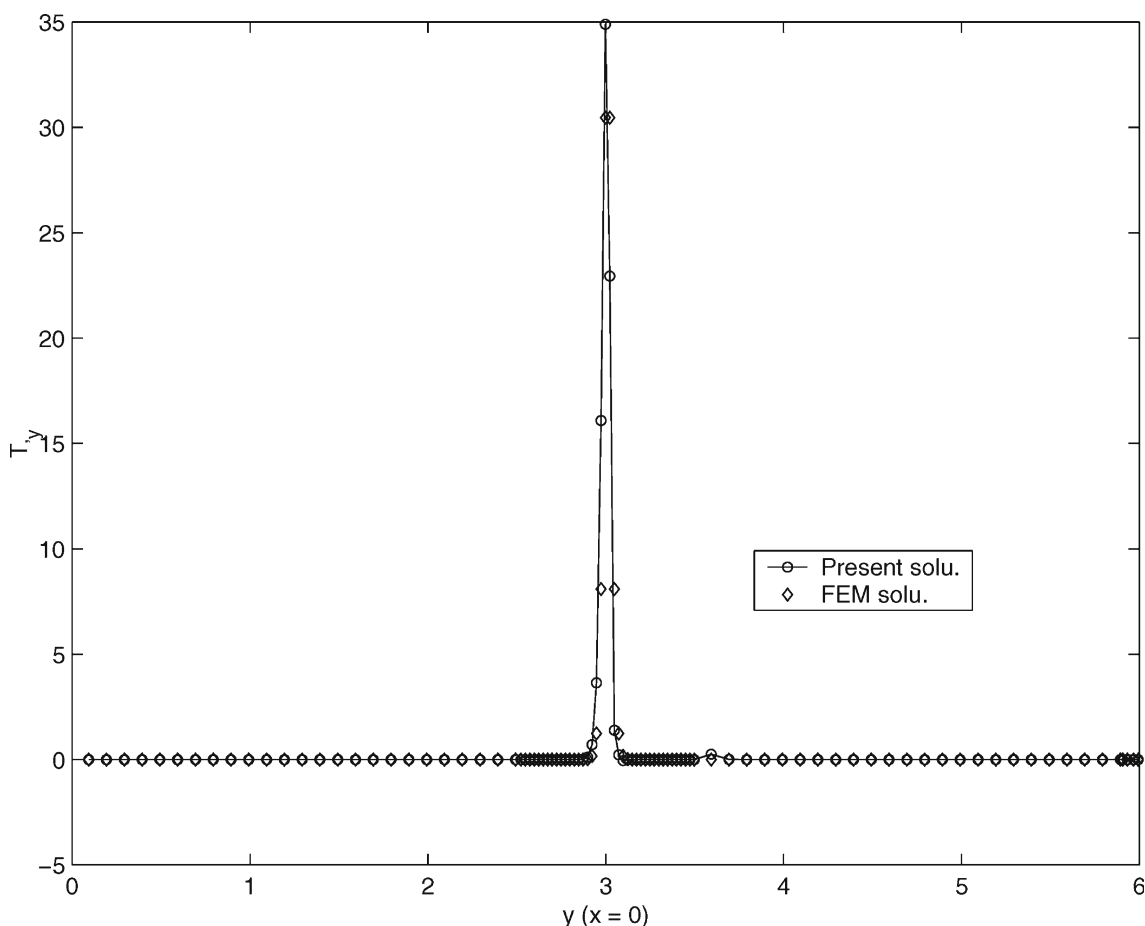


Fig. 15 Comparison between FEM and MLM-GI results of gradient field for the high-gradient problem

5. Dai KY, Liu GR, Lim KM, Gu YT (2003) Comparison between the radial point interpolation and the Kriging based interpolation used in mesh-free methods. *Comput Mech* 32:60–70
6. Gingold RA, Monaghan JJ (1977) Smooth particle hydrodynamics: theory and applications to non-spherical stars. *Man Not Roy Astron Soc* 181:375–289
7. Golberg MA, Chen CS, Bowman H (1999) Some recent results and proposals for the use of radial basis functions in the BEM. *Eng Anal Bound Elem* 23:285–296
8. Krongauz Y, Belytschko T (1997) Consistent pseudo-derivatives in meshless method. *Int J Numer Meth Engng* 146:371–386
9. Liszka T, Orkisz J (1980) The finite difference methods at arbitrary irregular grids and its applications in applied mechanics. *Comput Struct* 11:83–95
10. Liu GR (2002) *Mesh-free methods: moving beyond the finite element method*. CRC Press, Boca Raton, FL
11. Liu GR, Gu YT (2003) A mesh-free method: mesh-free weak-strong (MWS) form method for 2-D solids. *Comput Mech* 33:2–14
12. Liu GR, Han X (2003) *Computational inverse techniques in Non-destructive evaluation*. CRC Press, Boca Raton, FL
13. Liu GR, Liu MB (2003) *Smooth particle hydrodynamics: a mesh-free particle method*. World Scientific, New Jersey, NJ
14. Liu GR, Wu YL, Ding H (2004) Mesh-free weak-strong (MWS) form method and its application to incompressible flow problems. *Int J Numer Meth Fluids* 46:1025–1047
15. Liu WK, Jun S, Zhang YF (1995) Reproducing kernel particle methods. *Int J Numer Meth Fl* 20:1081–1106
16. Timoshenko SP, Goodier JN (1970) *Theory of elasticity*, 3rd edn. McGraw-Hill, New York, NY
17. Wang JG, Liu GR (2002a) A point interpolation meshless method based on radial basis functions. *Int J Numer Meth Eng* 54:1623–1648
18. Wang JG, Liu GR (2002b) On the optimal shape parameters of radial basis functions used for 2D meshless methods. *Comput Meth Appl Mech Eng* 191:2611–2630
19. Yoo JW, Moran B, Chen JS (2004) Stabilized conforming nodal integration in the natural-element method. *Int J Numer Meth Eng* 60:861–890